The Astrophysical Journal Letters, 951:L25 (7pp), 2023 July 10 https://doi.org/10.3847/2041-8213/acdd76
© 2023. The Author(s). Published by the American Astronomical Society.
OPEN ACCESS

Investigating Possible Binarity for GJ 229B

Alex R. Howe[1,2,3], Avi M. Mandell[1,4], and Michael W. McElwain[1]
[1] NASA Goddard Space Flight Center, 8800 Greenbelt Rd., Greenbelt, MD 20771, USA; alex.r.howe@nasa.gov
[2] Center for Research and Exploration in Space Science and Technology, NASA/GSFC, Greenbelt, MD 20771, USA
[3] Southeastern Universities Research Association, 1201 New York Avenue NW, Suite 430, Washington, DC 20005, USA
[4] GSFC Sellers Exoplanet Environments Collaboration, NASA/GSFC, Greenbelt, MD 20771, USA
Received 2022 November 15; revised 2023 June 9; accepted 2023 June 10; published 2023 July 7

Abstract

GJ 229B, the first type-T brown dwarf to be discovered, has presented a tension between comparisons with evolutionary models and the larger-than-expected mass and radius values derived from spectroscopic and astrometric observations. We examine the hypothesis that GJ 229B is actually a binary substellar object by using two grid-based fits using evolutionary models to explore the range of mass ratios of the possible binary components. We find that the best-fit component values are most consistent with a roughly 2:1 binary mass ratio and an age range of 2–6 Gyr. The observed temperatures, masses, and apparent radii match expected values from evolutionary models for a binary much better than a single-object model, but more detailed observations and modeling are needed to definitively confirm the binary hypothesis.

Unified Astronomy Thesaurus concepts: Brown dwarfs (185); T dwarfs (1679); Binary stars (154); Stellar atmospheres (1584)

1. Introduction

GJ 229B is noted for being the first type-T brown dwarf to be discovered (Nakajima et al. 1995),[5] with a measured effective temperature well below the L/T transition, ∼1200 K. Yet its atmospheric structure and composition have been less thoroughly studied than now-more-standard benchmark objects such as the similar GJ 570D (e.g., Line et al. 2015). This may be owing to its peculiar spectrum, which shows unusually weak H_2O and CH_4 features for its spectral type (Burgasser et al. 2006) and elevated levels of CO (Oppenheimer et al. 1998).

Dynamical measurements of the mass of GJ 229B have also yielded surprising results, with the most precise recent analysis finding a value of $71.4 \pm 0.6\,M_J$ (Brandt et al. 2021). This measurement was based on Gaia EDR3 data combined with several other astrometric and radial velocity data sets, resulting in an uncertainty significantly less than previous results. Yet it is incompatible with evolutionary models, as an object of that mass could not cool to the observed temperature of GJ 229B within a Hubble time. Meanwhile, an independent analysis of radial velocities alone found a minimum mass of only 1.62 M_J (Feng et al. 2020). Reconciling such a small minimum mass with the astrometric results requires fine-tuning the orbit solution with an orientation within ∼2° of face-on.

A newer analysis of the combined astrometric and radial velocity (RV) data set was undertaken with the addition of the Gaia–Hipparcos positional difference by Feng et al. (2022). This analysis found a dynamical mass for GJ 229B of $60.42^{+2.34}_{-2.38}\,M_J$. This mass is somewhat more plausible in terms of fitting evolutionary models. However, it still strongly precludes fitting the observed dynamical mass, effective temperature, and luminosity (and by proxy radius) simultaneously.

Recently, we undertook a spectroscopic retrieval study of GJ 229B's atmosphere with our APOLLO atmospheric retrieval framework (Howe et al. 2022), supplemented by an analysis incorporating the Sonora–Bobcat (S-B) grid of brown dwarf evolutionary models by Marley et al. (2017). This study showed that both spectroscopic retrieval measurements and evolutionary model fits return dramatically lower masses than the dynamical fits, with a retrieved mass estimate of $41.6 \pm 3.3\,M_J$. We also obtained an unexpectedly large radius estimate $1.105 \pm 0.025\,R_J$ (which is also implied by the luminosity and effective temperature of the object), which is inconsistent with evolutionary models of either mass, both of which predict a more compact object.

With such a large disparity in mass measurements, the most natural explanation would appear to be that GJ 229B is in fact a binary brown dwarf of unequal mass, with one component contributing most of the total flux to the spectrum, while the other contributes just enough flux to boost the apparent radius. This sort of discrepancy has been observed before for other objects, with binarity suggested as a solution to anomalously large retrieved radii (Line et al. 2017) and overall flux (Burgasser et al. 2008), so a similar solution seems likely for GJ 229B. In this Letter, we explore the possible parameter space for a binary GJ 229B using two different grid-fitting methods based on the S-B evolutionary models (Marley et al. 2017) and the APOLLO retrieval code, extending our analysis from Howe et al. (2022). First, we fit the observed spectrum of GJ 229B (Geballe et al. 1996; Noll et al. 1997; Schultz et al. 1998; Oppenheimer et al. 1998) to binary spectra derived from the S-B model grid directly. These atmosphere models are self-consistent, but do not account for the peculiar chemistry of GJ 229B or the supersolar C/O ratio found by Howe et al. (2022). Second, we generate a grid of APOLLO forward models for a binary object based on values for radius, gravity, and temperature structure from the S-B evolutionary tracks, but using our retrieved molecular abundances from Howe et al. (2022). For completeness, we consider

[5] Not to be confused with the Neptune-mass planet accompanying the host star, GJ 229Ab, sometimes written as GJ 229b (Tuomi et al. 2014).

Original content from this work may be used under the terms of the Creative Commons Attribution 4.0 licence. Any further distribution of this work must maintain attribution to the author(s) and the title of the work, journal citation and DOI.

fits using both the $M_{\rm tot} = 71\,M_J$ and $M_{\rm tot} = 60\,M_J$ dynamical mass measurements.

For each of these grids, we compute goodness-of-fit statistics for comparison to the observed spectrum of GJ 229B, and we find that both grid fits return qualitatively similar results. In the $M_{\rm tot} = 71\,M_J$ case, we find a primary mass of 51 M_J ($q = 0.39$) using both methods. The $M_{\rm tot} = 60\,M_J$ case shows modest differences, with $M_1 = 46\,M_J$ ($q = 0.30$) for S-B and $M_1 = 49\,M_J$ ($q = 0.22$) for APOLLO. Given this consistency between our two methods and the physical arguments against a single-object solution, we consider this to be significant evidence for a binary solution for this object.

The results from the two model grid fits are shown in Section 2, with an explanation of the limitations of our model in Section 3. We discuss the implications of our results in Section 4 and summarize our conclusions in Section 5. A full description of the data set we use in this paper is included in Howe et al. (2022).

2. Grid Fits Based on Evolutionary Models

We constructed two grids of spectra for binary brown dwarfs based on the solar-metallicity evolutionary tracks of the S-B model set (Marley et al. 2017). To create these spectra, we linearly interpolated the S-B tracks to a grid of 1 M_J in mass and 10 K in primary effective temperature. For each grid point in the resulting "S-B grid," we computed a primary spectrum and two secondary spectra by interpolating the nearest S-B spectra provided in the parameter space for two brown dwarfs of equal age and masses summing to 60 and 71 M_J. Likewise, for each grid point in the "APOLLO grid," we computed forward models using APOLLO for the same radii, surface gravities, and temperature profiles from the S-B models combined with our retrieved molecular abundances from Howe et al. (2022). Thus, we used the same evolutionary tracks for both grids, but two different, incomplete, but complementary chemistry models.

For each grid and each case (60 and 71 M_J), we summed the primary and secondary spectra together to create a grid of model binary spectra. We then computed the goodness of fit to the observed spectrum of GJ 229B using a reduced chi-squared statistic. We chose the reduced chi-squared statistic for this analysis for its relative simplicity. However, most other measures of goodness of fit such as the Bayesian likelihood, Bayesian information criterion, and APOLLO's own likelihood function produce virtually identical results because all of these measures are dominated by the error in the large number of spectral data points (which comprise nearly all of the >3200 degrees of freedom) rather than other statistical factors.

Heat maps of the reduced chi-squared results for both grids are shown in Figure 1 for the $M_{\rm tot} = 71\,M_J$ case and Figure 2 for the $M_{\rm tot} = 60\,M_J$ case, plotting primary effective temperature versus mass and age, as well as secondary effective temperature versus mass. All of the fits were found to have $\chi^2_\nu \geqslant 10$, but this is not an unexpected result given that we are not performing full retrievals (such as Markov Chain Monte Carlo retrievals) on the spectrum. To assess the uncertainties in these fits, we adopt 1σ errors of $\chi^2_\nu \leqslant 1.2\chi^2_{\nu,\rm min}$ based on an analysis of chi-squared statistics by Beringer et al. (2012; see their Figure 36.2 and associated chapter). We mark reduced chi-squared contours on the plots of $\chi^2_\nu = 11$, 12, and 13. Based on our definition, the outer contour is roughly equivalent to our 1σ uncertainties, although they are slightly different for each local minimum.

All four grid fits result in a relatively broad minimum in χ^2_ν spanning a width of ~15 M_J. For example, for the S-B model grid, our 1σ uncertainties in primary mass span 44–63 M_J in the 71 M_J case and 39–54 M_J in the 60 M_J case. In all cases, the primary effective temperature falls in a significantly narrower range of ~900–1000 K, which is consistent between the two total mass cases. Within each case, the S-B and APOLLO fits are qualitatively similar. However, the distribution for APOLLO forward models is broader in effective temperature and occurs at slightly lower temperatures overall. This is likely due to the chemistry model used for the APOLLO model grid, which assumes a constant atmospheric composition with respect to temperature, muting the effect of changing $T_{\rm eff}$ on the spectrum shape. Meanwhile, the realistic changes in chemistry in the S-B grid are likely to produce worse spectral fits at nonoptimal temperatures, as would be expected.

The parameters of the best fits from our model grids are listed in Tables 1 and 2 for the 71 and 60 M_J cases, respectively. We note that while the S-B grid has a single global minimum in reduced chi-squared, in both of our cases, the APOLLO grid produces three local minima along a line of increasing mass and temperature. For completeness, we list all three of the APOLLO minima for each case in Tables 1 and 2. These are compared with our best single-object free retrieval from Howe et al. (2022), and reduced chi-squared values are listed for all of the fits. Including the three APOLLO fits is also useful in that they are representative of our 1σ uncertainty distributions as a whole.

In Table 2, we also include single-object fits to both of our grids, subject to the same dynamical mass constraint of 60 M_J. These fits have higher reduced chi-squared values than the binary fits, so the binary solution is still favored in this case. For the 71 M_J case, the global minimum in χ^2_ν falls outside the distribution of allowed evolutionary models (and all models within the grid have very large $\chi^2_\nu > 10{,}000$), so we consider it to have no single-object solutions.

The most notable differences between the 60 and 71 M_J cases are in the mass ratio of the binary and the inferred age of the system. The 9 M_J difference in mass between the two cases is partitioned roughly equally between the primary and secondary mass, with the overall effect being a significantly more extreme mass ratio in the 60 M_J case. The S-B best fit (which in both cases is also representative of the APOLLO best fits) in the 71 M_J case has a mass partition of 51 and 20 M_J for a mass ratio of $q = 0.392$. In the 60 M_J case, the mass partition is 46 and 14 M_J, with $q = 0.304$. Given a smaller total mass, a smaller primary mass with nearly the same $T_{\rm eff}$ has a larger radius and thus produces a larger fraction of the total flux of the binary, so a cooler and lower-mass secondary is needed to make up the difference.

Likewise, a lower-mass primary would need a shorter time to cool to the same $T_{\rm eff}$, resulting in a younger inferred age of the system. For the S-B best fit, the difference is about 1 Gyr, reducing from 4.5 Gyr in the 71 M_J case to 3.5 Gyr in the 60 M_J case. All of the fits listed in Tables 1 and 2 fall in the range of 2.6–6.1 Gyr, somewhat older than previous estimates (e.g., Nakajima et al. 2015).

As a representative example of the spectra resulting from our grid fits, Figure 3 compares the best-fit spectra from each grid (blue and gold) and their residuals (green and red) with the

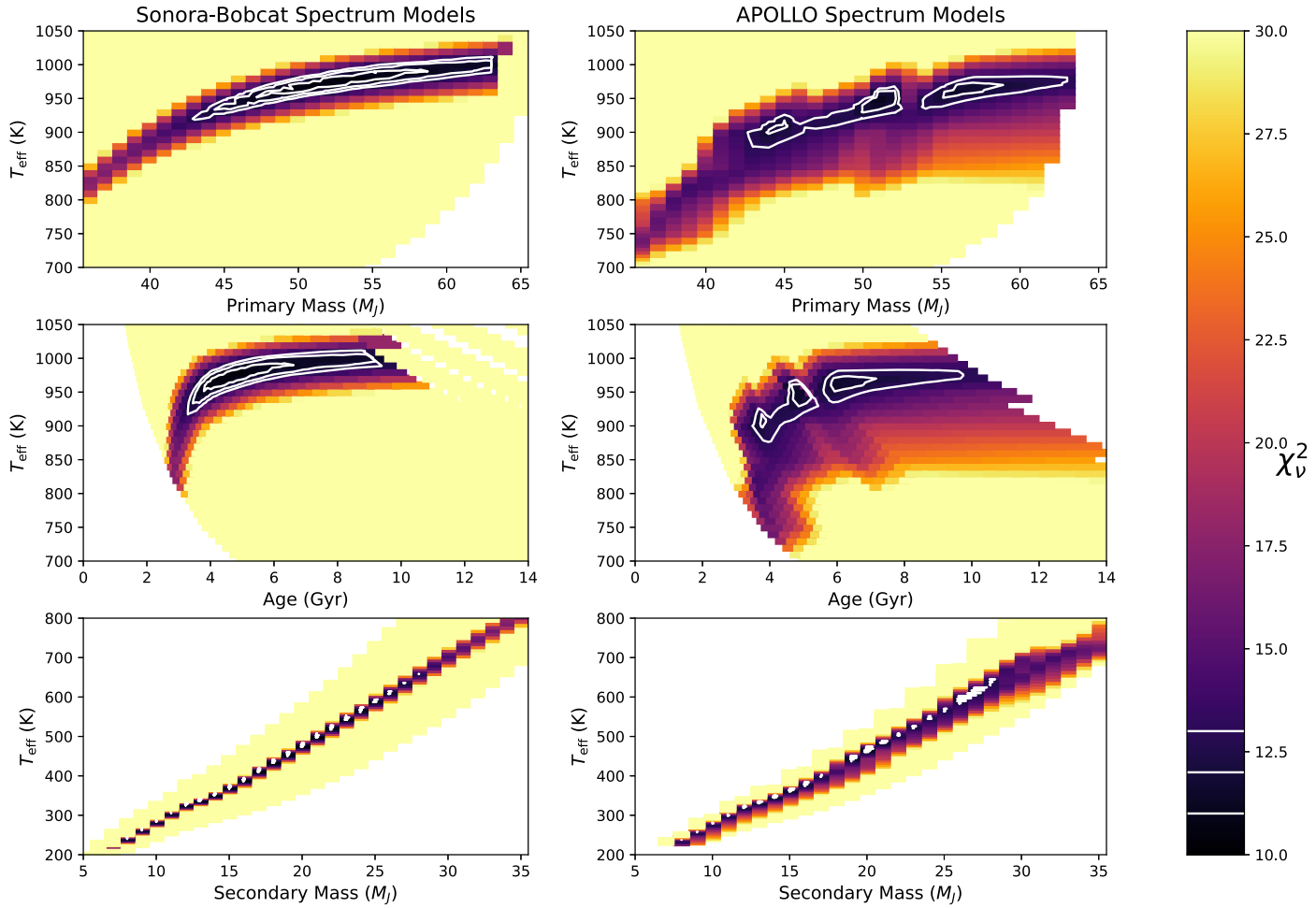

Figure 1. Goodness of fit to observed spectra of GJ 229B of our binary forward model grids, with a total mass of 71 M_J, calculated from the Sonora–Bobcat (S-B) models (Marley et al. 2017) (left) and from out APOLLO forward models (right). For the primary, the cutoff on the left edge is based on a mass greater than 50% of the total mass of the system, and the cutoff on the right is based on an age less than a Hubble time. For the secondary, the low temperature cutoff is based on the limitations of the molecular cross-section tables used by APOLLO. The outermost contours are representative of our adopted 1σ uncertainties, although they are slightly different for each local minimum.

observed spectrum of GJ 229B in the 71 M_J case. Both grid fits match the observed spectrum at many wavelengths; however, they both show errors in different wavelength ranges. The S-B fit shows significant residuals in the J and M bands, while the APOLLO fit shows significant residuals mainly in the Y and K bands. Note that features in the residual spectra are exaggerated in regions of low observational uncertainties, so their magnitude is more indicative of the observational precision than actual absorption features.

3. Limitations of the Model

The S-B model set provides a complete grid of spectra only for brown dwarf models of solar metallicity and C/O ratio. Therefore, a detailed grid fit to an observed spectrum must make compromises with regard to the chemistry. Our S-B grid fit to GJ 229B assumes an essentially solar composition, which is inconsistent with both the peculiar spectrum of this object and the retrieved molecular abundances from Howe et al. (2022). Our measured supersolar C/O ratio of 1.13 is consistent with other retrievals of T dwarfs (e.g., Line et al. 2015), but is well outside the a priori parameters of generic brown dwarf model sets such as S-B.

Additionally, the temperature–pressure (T-P) profiles in both forward model grids are interpolated from the S-B models. They are not informed by our retrieved T-P profile from Howe et al. (2022), and in the context of the grid, it is de facto a two-parameter model controlled only by $T_{\rm eff}$ and log g. This is analogous to the parametric T-P profile used in Howe et al. (2022), which we found to return relatively poor goodness-of-fit statistics, even in a full ensemble retrieval.

Meanwhile, our APOLLO grid assumes a constant molecular composition for brown dwarfs of different temperatures, as a full thermochemical model of the atmosphere is beyond the scope of APOLLO, which is designed around a free retrieval philosophy for a single object. Therefore, neither of the model grids used in this analysis fully simulate the atmospheric chemistry of GJ 229B. A fully self-consistent chemical model with supersolar C/O would be needed to model the spectrum of a binary brown dwarf to a greater accuracy than we have done in this paper.

The limitations of the chemical model for the APOLLO grid are especially significant for the secondary spectrum, which is much cooler than the effective temperature retrieved for a single-object fit. Thus, the atmospheric chemistry is expected to be quite different from our assumed abundances. In performing

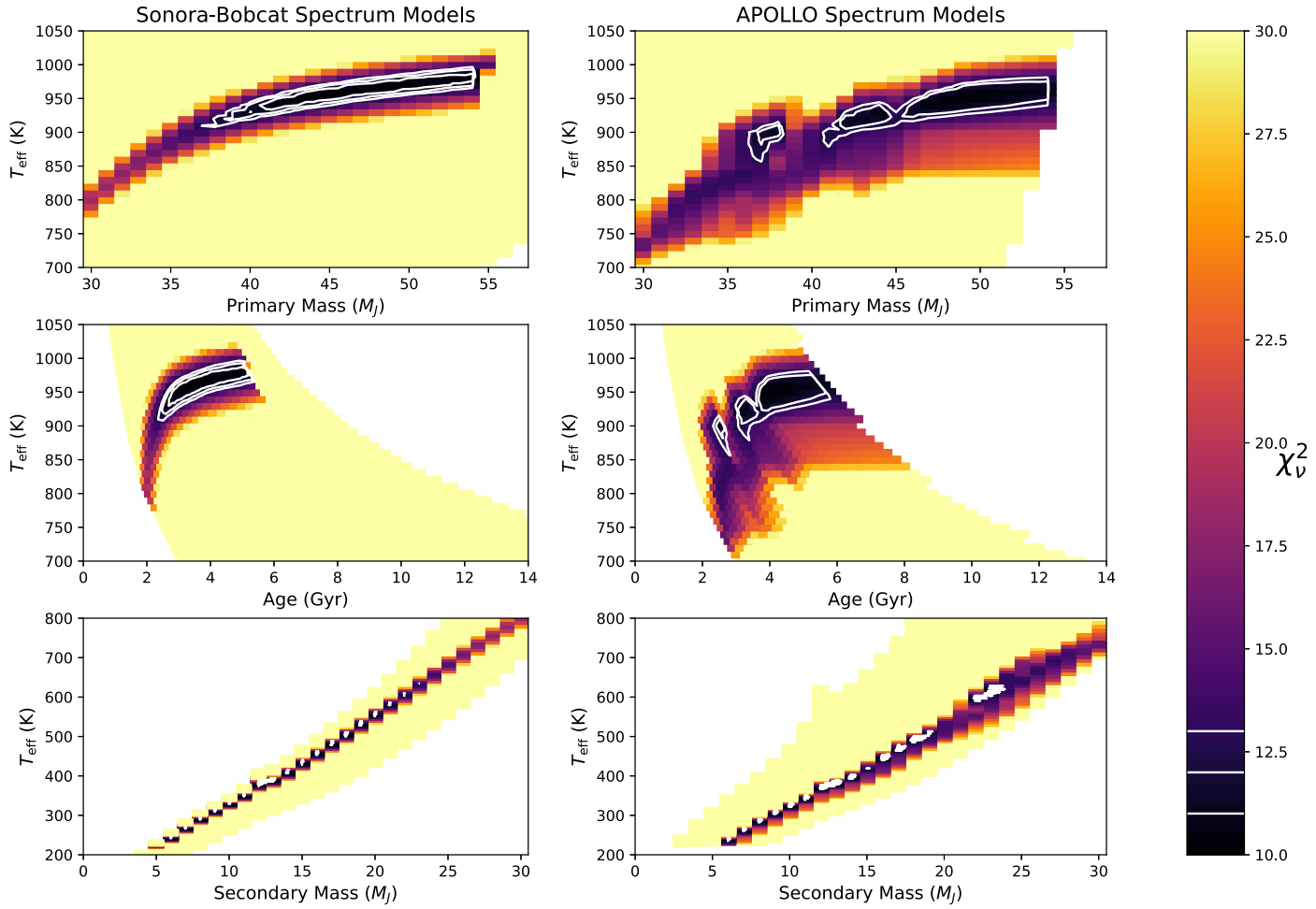

Figure 2. Same as Figure 1, except with a total mass of 60 M_J.

Table 1
The Best-fit Binary Models from the Sonora–Bobcat (S-B) Model Set and Our APOLLO Forward Model Grid with a Total Mass of 71 M_J

	Binary				Single		
	S-B	APOLLO 1[a]	APOLLO 2[a]	APOLLO 3	S-B	APOLLO	Free Retrieval
Primary Mass (M_J)	51^{+12}_{-7}	45^{+8}_{-3}	51^{+1}_{-8}	56^{+6}_{-2}	No Solution	No Solution	41.6 ± 3.3
Primary $T_{\rm eff}$ (K)	970^{+40}_{-50}	910 ± 60	950^{+20}_{-80}	960 ± 30			869^{+5}_{-7}
Primary Radius (R_J)	$0.811^{+0.040}_{-0.045}$	$0.833^{+0.009}_{-0.033}$	$0.809^{+0.033}_{-0.007}$	$0.788^{+0.008}_{-0.026}$			1.105 ± 0.025
Primary log g	$5.30^{+0.15}_{-0.12}$	$5.23^{+0.09}_{-0.05}$	$5.31^{+0.01}_{-0.11}$	$5.37^{+0.08}_{-0.02}$			$4.93^{+0.02}_{-0.03}$
Secondary Mass (M_J)	20^{+7}_{-12}	26^{+3}_{-8}	20^{+8}_{-1}	15^{+2}_{-6}			
Secondary $T_{\rm eff}$ (K)	478^{+210}_{-216}	596^{+77}_{-164}	469^{+176}_{-32}	364^{+38}_{-130}			
Secondary Radius (R_J)	$0.940^{+0.069}_{-0.039}$	$0.909^{+0.036}_{-0.013}$	$0.938^{+0.006}_{-0.040}$	$0.972^{+0.036}_{-0.019}$			
Secondary log g	$4.77^{+0.20}_{-0.46}$	$4.91^{+0.08}_{-0.17}$	$4.77^{+0.18}_{-0.03}$	$4.61^{+0.08}_{-0.30}$			
Mass Ratio (M_2/M_1)	$0.392^{+0.221}_{-0.265}$	$0.578^{+0.212}_{-0.238}$	$0.392^{+0.298}_{-0.027}$	$0.268^{+0.047}_{-0.122}$			
Flux Ratio (F_2/F_1)	$0.079^{+0.224}_{-0.070}$	$0.219^{+0.073}_{-0.135}$	$0.080^{+0.166}_{-0.001}$	$0.031^{+0.012}_{-0.025}$			
Age (Gyr)	$4.5^{+4.7}_{-1.4}$	$3.8^{+1.8}_{-0.5}$	$4.8^{+0.7}_{-1.4}$	$6.1^{+4.0}_{-0.6}$			>1.0
χ^2_ν	10.37	11.81	11.14	11.54			8.15

Note. Bolometric flux ratios are calculated from the Stephan–Boltzmann law. The retrieved parameters are compared with our best-fit free retrieval for a single object (Howe et al. 2022). No solutions for a single object with a global χ^2_ν minimum lie within either of the model grids, which we interpret as having no solution with physically plausible parameters. Uncertainties are defined by $\chi^2_\nu \leqslant 1.2\chi^2_{\nu,\rm min}$ based on an analysis by Beringer et al. 2012.
[a] The APOLLO 1 and APOLLO 2 models are two peaks of a shared 1σ distribution.

the fits with the APOLLO grid, we assume that the relatively smaller flux from the secondary means that it will produce a proportionately smaller error in the overall spectrum.

An additional limitation of the APOLLO-based grid was the inability of APOLLO to model atmospheres of very cold (old and low-mass) secondaries due to the low-temperature limits of

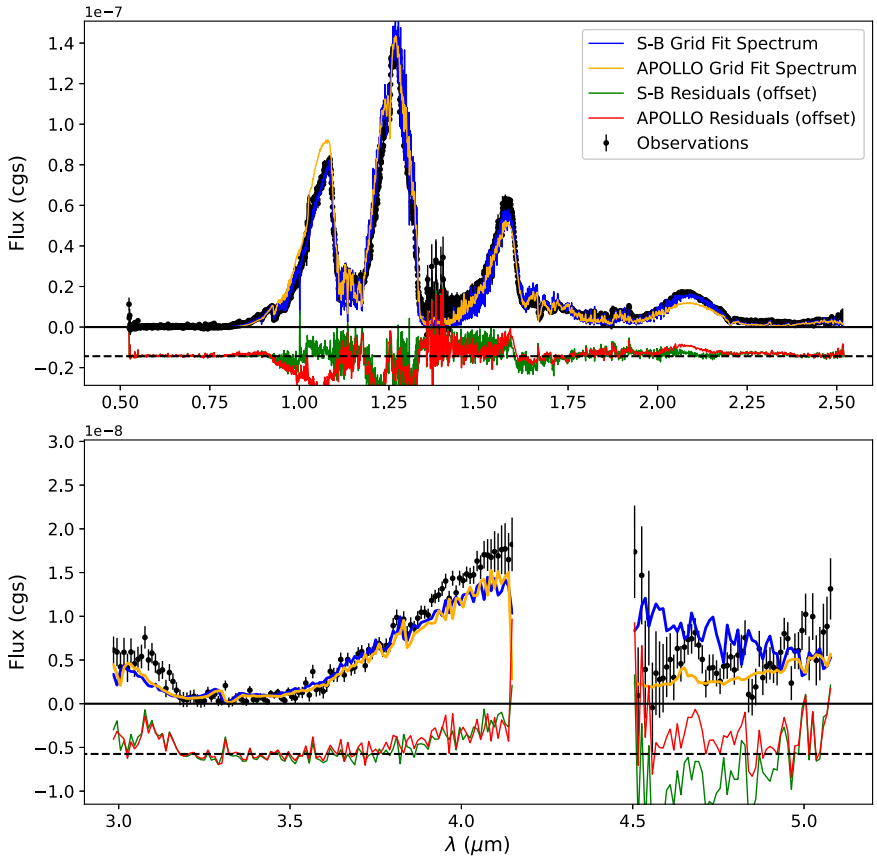

Figure 3. Comparison of the observed spectrum of GJ 229B (black) with best-fit binary spectra from the S-B model grid (blue) and our APOLLO forward model grid (gold), in the 71 M_J case. Residuals for each fit are plotted on the same scale below the x-axis in green and red, respectively.

Table 2
Same As Table 1, Except with a Total Mass of 60 M_J

	Binary				Single		
	S-B	APOLLO 1	APOLLO 2	APOLLO 3	S-B	APOLLO	Free Retrieval
Primary Mass (M_J)	46^{+8}_{-7}	$38^{+0.5}_{-2}$	44^{+1}_{-3}	49^{+5}_{-3}	60	60	41.6 ± 3.3
Primary $T_{\rm eff}$ (K)	960^{+30}_{-40}	900^{+20}_{-50}	930^{+10}_{-50}	950 ± 30	1000^{+10}_{-20}	970 ± 20	869^{+5}_{-7}
Primary Radius (R_J)	$0.835^{+0.061}_{-0.033}$	$0.872^{+0.011}_{-0.002}$	$0.841^{+0.013}_{-0.003}$	$0.818^{+0.014}_{-0.023}$	$0.777^{+0.001}_{-0.002}$	$0.773^{+0.003}_{-0.002}$	1.105 ± 0.025
Primary log g	$5.23^{+0.13}_{-0.18}$	$5.11^{+0.01}_{-0.08}$	$5.21^{+0.01}_{-0.05}$	$5.28^{+0.06}_{-0.04}$	5.412 ± 0.002	5.416 ± 0.003	$4.93^{+0.02}_{-0.03}$
Secondary Mass (M_J)	14^{+7}_{-8}	$22^{+2}_{-0.5}$	16^{+3}_{-1}	11^{+3}_{-5}			
Secondary $T_{\rm eff}$ (K)	411^{+174}_{-169}	597^{+38}_{-7}	449^{+64}_{-30}	346^{+56}_{-108}			
Secondary Radius (R_J)	$0.990^{+0.059}_{-0.051}$	$0.944^{+0.002}_{-0.018}$	$0.975^{+0.002}_{-0.021}$	$1.011^{+0.028}_{-0.024}$			
Secondary log g	$4.57^{+0.30}_{-0.50}$	$4.81^{+0.11}_{-0.01}$	$4.64^{+0.09}_{-0.07}$	$4.45^{+0.12}_{-0.29}$			
Mass Ratio (M_2/M_1)	$0.304^{+0.234}_{-0.193}$	$0.579^{+0.088}_{-0.021}$	$0.364^{+0.100}_{-0.030}$	$0.224^{+0.080}_{-0.113}$			
Flux Ratio (F_2/F_1)	$0.047^{+0.120}_{-0.031}$	$0.227^{+0.036}_{-0.001}$	$0.073^{+0.116}_{-0.006}$	$0.027^{+0.017}_{-0.020}$			
Age (Gyr)	$3.5^{+1.8}_{-1.0}$	2.6 ± 0.3	$3.4^{+0.2}_{-0.4}$	$4.3^{+1.4}_{-0.6}$	$7.0^{+0.4}_{-0.2}$	$7.7^{+0.5}_{-0.4}$	>1.0
χ^2_ν	9.97	11.22	10.92	10.25	11.25	24.56	8.15

Note. Single-object solutions for both grid fits are listed alongside the free retrieval from Howe et al. (2022).

our molecular optical cross-section tables. This prevented us from fully exploring the parameter space at ages $\gtrsim$10 Gyr in the 71 M_J case and $\gtrsim$6 Gyr in the 60 M_J. However, the contour plots in Figures 1 and 2 indicate that the best-fit models are clustered at younger ages in the region of the parameter space we did explore.

The reduced chi-squared values for our grid fits in this work are consistently significantly larger than that of our free retrieval of the single-object solution for GJ 229B in Howe et al. (2022). We attribute this to our less accurate treatment of the chemistry in both model grids, as described above, and to the simplified T-P profiles. The goodness of fit when performing a free retrieval using a parametric T-P profile was comparable to that of our grid fits in this work, which may be a result of both models being underdetermined to fully fit the observed spectrum.

We do not attempt a full retrieval of the prospective binary spectrum in this work, as would be required to make an accurate comparison of the goodness of fit between the single and binary models. The number of variables involved in retrieving properties of two independent objects from a blended spectrum is prohibitive and beyond the scope of the current version of APOLLO, and a free retrieval on a blended spectrum would likely have too many degeneracies to produce unambiguous results. Again, a full chemical model for a binary object would be needed to constrain the parameter space.

Nonetheless, we see that both of our grid fits produce similar results for best fits in M–$T_{\rm eff}$ space, and they also fit complementary wavelength regimes of the observed spectrum. The consistency of this result across two methods emphasizing different chemistry increases our confidence in the viability of our method to infer the properties of a binary brown dwarf in this context.

4. Discussion

4.1. Physical Argument for a Binary Solution

Our investigation of binarity for GJ 229B was motivated by multiple lines of evidence that render a single-object solution improbable, if not outright unphysical, given our current understanding of brown dwarf evolution. First, the combination of observed luminosity and effective temperature, even prior to dynamical mass measurements, implies an unusually large radius for a single object. Our single-object retrieval in Howe et al. (2022) found a radius of 1.105 ± 0.025 R_J. When combined with our retrieved $T_{\rm eff} = 869^{+5}_{-7}$ K, based on the S-B models, this suggests a very young and low-mass object with an age of <0.5 Gyr and a mass near the deuterium-burning limit.

While this solution could fit the luminosity and effective temperature of GJ 229B, it is wildly inconsistent with the very large dynamical mass measurements made in recent years. A massive brown dwarf of 71 M_J would not be able to cool to the observed temperature of GJ 229B in a Hubble time, and the S-B evolutionary tracks include no valid solutions for GJ 229B with this mass. A 60 M_J brown dwarf could cool sufficiently in $\sim$7–10 Gyr. However, these solutions still fail with high confidence to replicate our retrieved radius, setting an upper bound of $R \leqslant 0.77\,R_J$. In contrast, a binary object with an unequal flux ratio would replicate the apparent oversized radius much more easily.

4.2. Inferred Mass Ratio of GJ 229B in the Context of Other Brown Dwarf Binaries

Our inferred mass ratio for a potential binary GJ 229B is notable in that it is fairly unequal, with a best-fit solution of $q = 0.39$ in the 71 M_J case for both grid fits and an even more extreme $q = 0.30$ in the 60 M_J case for the S-B fit (albeit with large uncertainties). In contrast, the most notable well-constrained dynamical mass ratios measured for binary brown dwarfs are all near $q \sim 0.8$ (Chen et al. 2022; Bedin et al. 2017; Zapatero Osorio et al. 2004). However, inferred mass ratios for other binaries based on evolutionary models are more varied, with several estimated to be near $q \sim 0.5$ (Faherty et al. 2020; Gonzales et al. 2020; Reiners et al. 2010).

Population-level studies of brown dwarf binaries are subject to greater systematic uncertainties because dynamical masses are generally not available, forcing them to rely on evolutionary models and mass–luminosity relations. Early population studies along these lines yielded conflicting results. Burgasser et al. (2003) did a survey of T dwarf binaries and found significant numbers of systems down to $q \sim 0.4$, based on a mass–luminosity relation. However, in a later study, Burgasser et al. (2007) estimated 77% of very-low-mass (VLM; $<0.1\,M_\odot$) binaries have $q \geqslant 0.8$; but this study reported low completeness for unequal ratios of $q \leqslant 0.6$, and their best-fit model suggested that mass ratios as low as $q \sim 0.4$ may be plausible for VLM binaries. In a later study, Dupuy & Liu (2017) measures mass ratios for 19 binary brown dwarfs and found that most of them had $q \gtrsim 0.8$, and all of them had $q \gtrsim 0.6$.

These population studies do not show strong evidence for highly unequal binary brown dwarf mass ratios. However, some of them do extrapolate the binary brown dwarf population to be consistent with a mass ratio for GJ 229B of $q = 0.39$. More promising is that the uncertainties in our analysis allow a much more equal mass ratio, reaching as high as $q = 0.79$ for the APOLLO 1 fit in the 71 M_J case. This indicates that there are a significant number of solutions that are consistent with population studies, so this is not a large obstacle to a binary interpretation for GJ 229B.

4.3. Detectability of a Binary

The definitive proof of binarity for this object would of course be direct observation, either by resolving the separate components, or by observing the reflex motion of the primary. At least one and possibly both of these methods should be able to significantly constrain the parameters of the binary. At a distance of 5.76 pc, the fact that the two components are not resolved in Hubble Space Telescope images (Nakajima et al. 1995) suggests that their projected separation is <0.5 au. However, we note that adaptive optics measurements with ground-based telescopes stand a fair chance of being able to resolve the components or measure the motion of the centroid. Typical adaptive optics systems will offer a resolution as small as $\sim$0.2 au at that distance, and the GRAVITY instrument on the Very Large Telescope may be able to resolve 1 order of magnitude closer (GRAVITY Collaboration et al. 2017). As for radial velocity characterization, the apparent face-on orientation of the system as a whole as derived from astrometry suggests that any signal may be weak. However, if the orbit of the binary is significantly tilted relative to their mutual orbit around GJ 229A, their orbital motion at such small separations (at least several kilometers per second for the primary) should be well within the capability of ground-based spectroscopy.

For both of the most recent dynamical mass measurements of GJ 229B, none of the S-B evolutionary models can replicate the dynamical mass, effective temperature, and luminosity simultaneously for a single object, whereas a binary solution does so quite easily. Therefore, we feel confident in proposing it as a viable solution to the puzzles surrounding this object. We further note that our binary fits consistently predict an older age range for the system of 2–6 Gyr. In the absence of direct dynamical or spectroscopic evidence for binarity, an asteroseismic age measurement of GJ 229A could help to further constraint the parameter space for a binary brown dwarf companion.

5. Conclusions

Both spectroscopic retrievals and spectral energy distribution considerations combined with evolutionary models consistently suggest a smaller mass for the late T dwarf GJ 229B than the dynamical mass of $71.4 \pm 0.6\,M_J$ (Brandt et al. 2021), or $60.42^{+2.34}_{-2.38}\,M_J$ (Feng et al. 2022), suggesting that it may be a binary object. We have employed grid-based methods using the S-B evolutionary models (Marley et al. 2017) and the APOLLO retrieval code (Howe et al. 2022) to estimate the mass ratio of a prospective binary GJ 229Ba and Bb. Our best-fit solutions for the S-B grid fits (which have the smallest reduced chi-squared values) give a mass ratio of $0.39^{+0.22}_{-0.27}$ for the 71 M_J case and $0.30^{+0.23}_{-0.19}$ for the 60 M_J case. While these ratios are fairly unequal, they do overlap with the ranges inferred for resolved brown dwarf binaries from some population studies. These fits are also consistent with an intermediate age range for the system of 2–6 Gyr.

There is a significant probability that precise astrometric and/or radial velocity measurements will be able to confirm the binarity of GJ 229B. In the absence of such measurements, a blended spectrum retrieval incorporating an equilibrium chemistry model may be able to significantly refine the mass ratio estimated in this work.

Acknowledgments

A.R.H. was supported by an appointment to the NASA Postdoctoral Program at NASA Goddard Space Flight Center, administered by Oak Ridge Associated Universities under contract with NASA. A.R.H. also acknowledges support by NASA under award No. 80GSFC21M0002 through the CRESST II cooperative agreement. A.M.M. acknowledges support from GSFC Sellers Exoplanet Environments Collaboration (SEEC), which is funded in part by the NASA Planetary Science Divisions Internal Scientist Funding Model. This work was partially supported by the GSFC Exoplanets Spectroscopy Technologies (ExoSpec), which is part of the NASA Astrophysics Science Division's Internal Scientist Funding Model. We thank Beth Biller and Robert Haring-Kaye for helpful conversations. We also thank the anonymous referee, whose commentary has signficantly improved the thoroughness and clarity of this paper.

ORCID iDs

Alex R. Howe https://orcid.org/0000-0002-4884-7150
Avi M. Mandell https://orcid.org/0000-0002-8119-3355
Michael W. McElwain https://orcid.org/0000-0003-0241-8956

References

Bedin, L. R., Pourbaix, D., Apai, D., et al. 2017, MNRAS, 470, 1140
Beringer, J., Arguin, J. F., Barnett, R. M., et al. 2012, PhRv, 86, 010001
Brandt, G. M., Dupuy, T. J., Li, Y., et al. 2021, AJ, 162, 301
Burgasser, A. J., Geballe, T. R., Leggett, S. K., Kirkpatrick, J. D., & Golimowski, D. A. 2006, ApJ, 637, 1067
Burgasser, A. J., Kirkpatrick, J. D., Reid, I. N., et al. 2003, ApJ, 586, 512
Burgasser, A. J., Reid, I. N., Siegler, N., et al. 2007, in Protostars and Planets V, ed. B. Reipurth, D. Jewitt, & K. Keil (Tuscon, AZ: Univ. Arizona Press), 427
Burgasser, A. J., Tinney, C. G., Cushing, M. C., et al. 2008, ApJL, 689, L53
Chen, M., Li, Y., Brandt, T. D., et al. 2022, AJ, 163, 288
Dupuy, T. J., & Liu, M. C. 2017, ApJS, 231, 15
Faherty, J. K., Goodman, S., Caselden, D., et al. 2020, ApJ, 889, 176
Feng, F., Butler, R. P., Shectman, S. A., et al. 2020, ApJS, 246, 11
Feng, F., Butler, R. P., Vogt, S. S., et al. 2022, ApJS, 262, 21
Geballe, T. R., Kulkarni, S. R., Woodward, C. E., & Sloan, G. C. 1996, ApJL, 467, L101
Gonzales, E. C., Burningham, B., Faherty, J. K., et al. 2020, ApJ, 905, 46
GRAVITY Collaboration, Abuter, R., Accardo, M., et al. 2017, A&A, 602, A94
Howe, A. R., McElwain, M. W., & Mandell, A. M. 2022, ApJ, 935, 107
Line, M. R., Teske, J., Burningham, B., Fortney, J. J., & Marley, M. S. 2015, ApJ, 807, 183
Line, M. R., Marley, M. S., Liu, M. C., et al. 2017, ApJ, 848, 83
Marley, M. S., Saumon, D., Fortney, J. J., et al. 2017, AAS Meeting, 230, 315
Nakajima, T., Oppenheimer, B. R., Kulkarni, S. R., et al. 1995, Natur, 378, 463
Nakajima, T., Tsuji, T., & Takeda, Y. 2015, AJ, 150, 53
Noll, K. S., Geballe, T. R., & Marley, M. S. 1997, ApJL, 489, L87
Oppenheimer, B. R., Kulkarni, S. R., Matthews, K., & van Kerkwijk, M. H. 1998, ApJ, 502, 932
Reiners, A., Seifahrt, A., & Dreizler, S. 2010, A&A, 513, L9
Schultz, A. B., Allard, F., Clampin, M., et al. 1998, ApJL, 492, L181
Tuomi, M., Jones, H. R. A., Barnes, J. R., Anglada-Escudé, G., & Barnes, J. S. 2014, MNRAS, 441, 1545
Zapatero Osorio, M. R., Lane, B. F., Pavlenko, Y., et al. 2004, ApJ, 615, 958